URSI GASS 2021, Rome, Italy, 28 August - 4 September 2021

Quantitative Microwave Imaging of Flattened Breast Phantoms with Direct Inversion Algorithms

Natalia K. Nikolova[(1)], Daniel Tajik[(1)], Romina Kazemivala[(1)], and Michael D. Noseworthy[(2)]
(1) Department of Electrical and Computer Engineering, McMaster University, Canada
(2) School of Biomedical Engineering, McMaster University, Hamilton, Canada

Abstract

We demonstrate the imaging of flattened breast phantoms with recently proposed quantitative real-time reconstruction methods that work with microwave *S*-parameter measurements, namely, quantitative microwave holography (QMH) and scattered-power mapping (SPM). The data is acquired in the frequency band from 3 GHz to 8 GHz. The comparison with X-ray computed tomography (CT) images indicates that diagnostic information is clearly present in the images produced by the microwave modality. Despite their lower spatial resolution in comparison with CT, the microwave images correctly localize mock cancers of 1-cm^3 size in both the real and the imaginary parts of the complex permittivity.

1 Introduction

The use of microwaves in medical diagnostics has been a major pursuit of the research community over the last half century [1]–[3]. The low equipment and maintenance costs are key advantages over both MRI and CT. Furthermore the nonionizing nature of microwave radiation is important when comparing against X-ray modalities, especially in applications requiring frequent examinations, e.g., breast-cancer screening. Although the modality's spatial resolution is only on the order of a centimeter, it is deemed sufficient for mass screening. However, microwave imaging is yet to prove sufficient sensitivity and specificity in clinical trials.

2 Real-time Quantitative Imaging

Quantitative microwave holography (QMH) and scattered-power mapping (SPM) are two recently proposed methods for quantitative image reconstruction in real time. Both exploit a measured system-specific point-spread function (PSF) to construct the forward model of scattering in terms of *S*-parameters. Importantly, this model proves accurate in near-field imaging, which is the case in tissue imaging.

The PSF-based model is then inverted efficiently in Fourier (or *k*-space) with reconstruction times on the order of seconds. The inversion strategies of QMH and SPM are fundamentally different. From a mathematical standpoint, what distinguishes the two methods is that QMH performs data matching at each point in the data *k*-space whereas SPM does so by minimizing the ℓ_2 norm of the data error in the entire data space. Details can be found in [3]-[6].

Table 1. Averaged permittivity of phantom materials from 3 GHz to 8 GHz.

Material	ε'	ε''
Carbon-rubber sheet	10.91	2.84
Matching medium	10.41	5.07
Simulated tumour	55.27	16.63
Simulated fibroglandular tissue	23.83	11.27

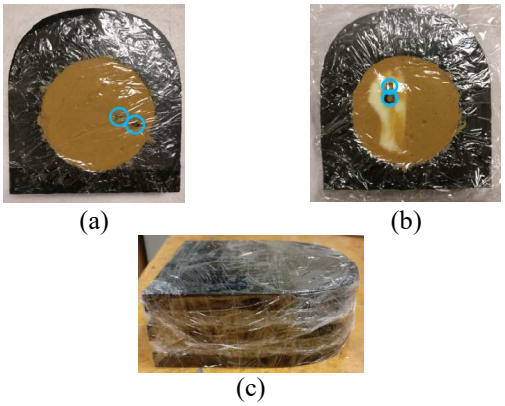

Figure 1. Photos of the compressed breast phantom: (a) Layer 2, (b) Layer 4, (c) complete phantom. Images adapted from [9].

3 Experimental Setup

The data is acquired with a planar raster scanning system, where, at each spatial position, a vector network analyzer (VNA) sweeps the frequency range from 3 GHz to 8 GHz in 100 MHz increments. The VNA is equipped with an RF switch allowing for the use of 1 transmitting (Tx) antenna [7] and 9 receiving antennas in a fixed arrangement for transmission measurements. The central element of the 9-element Rx bowtie array [8] is aligned with the boresight of the Tx TEM horn, which resides at the opposite side of the flattened breast phantom. The translation stage moves the phantom laterally between the antennas.

The lateral scan along *x* and *y* covers a 141 mm by 141 mm area with 3 mm increments. Photos of the breast tissue phantom are shown in Fig. 1. Table I shows the permittivity values of the different phantom constituents. The phantom is constructed from five 11 mm carbon-rubber sheets designed to match the permittivity of averaged scattered fibroglandular breast tissue. The second and fourth layers have sections removed, allowing for additional "healthy" and "cancer tissue" simulants to be inserted. In Layer 2, the cavity is filled with a "matching" medium, the permittivity

of which is close to that of the carbon-rubber sheets. Two tumor simulants of approximate size of 10 mm are also inserted so that they touch. Layer 4 contains not only "matching" medium but also fibroglandular tissue simulant along with two tumor simulants of the same size as in Layer 2. These simulants, too, are placed next to each other. All five layers are stacked and wrapped in plastic wrap.

4 Microwave and CT Images

Fig. 2 shows microwave quantitative images produced by QMH. The images are 2-dimensional (2D), similarly to mammography. They can be understood as projections of the 3D permittivity distribution in the lateral plane. The fibroglandular and tumor tissues are quantitatively estimated and identified well in the real-permittivity image. The imaginary-permittivity image is particularly successful in identifying the tumor simulants, which have significantly higher conductivity than the rest of the tissue phantom. The individual tumor simulants are not well separated due to the resolution limit of the system estimated at approximately 10 mm [6].

Fig. 3 shows slices of the 3D CT image coinciding with Layers 2 and 4. All structures are identified, including the air pockets which were not removed well during the construction of the tissue phantom. This is expected as the spatial resolution of CT (0.5 mm to 0.6 mm) [11] is markedly superior to all other imaging modalities, MRI included. The CT contrast between "cancers" and surrounding media is relatively low but sufficient to identify the phantom constituents.

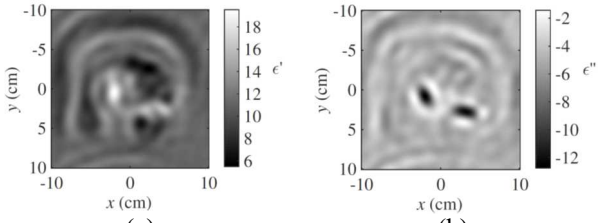

(a) (b)

Figure 2. QMH reconstruction of the breast phantom. All layers of the phantom are superimposed into one image due to the 2D reconstruction. (a) Real part of the permittivity. (b) Imaginary part of the permittivity.

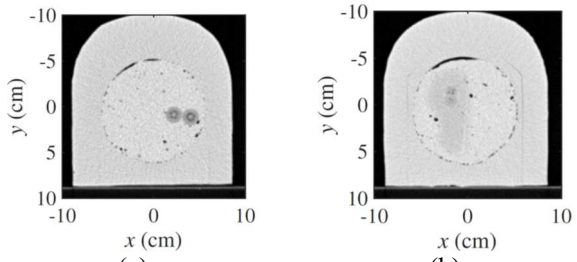

(a) (b)

Figure 3. CT image slices of the breast phantom at: (a) Layer 2; (b) Layer 4. Adapted from [10].

5 References

1. N. K. Nikolova, "Microwave imaging for breast cancer," *IEEE Microwave Mag*., vol. 12, no. 7, pp. 78–94, Dec. 2011, doi: 10.1109/MMM.2011.942702.

2. D. O'Loughlin, M. O'Halloran, B. M. Moloney, M. Glavin, E. Jones, and M. A. Elahi, "Microwave breast imaging: clinical advances and remaining challenges," *IEEE Trans. Biomed. Eng*., vol. 65, no. 11, pp. 2580–2590, Nov. 2018, doi: 10.1109/TBME.2018.2809541.

3. N.K. Nikolova, *Introduction to Microwave Imaging*. Cambridge University Press, July 2017.

4. D. Tajik, F. Foroutan, D. S. Shumakov, A. D. Pitcher, and N. K. Nikolova, "Real-time microwave imaging of a compressed breast phantom with planar scanning," *IEEE J. Electromagnetics, RF and Microwaves in Medicine and Biology*, vol. 2, no. 3, pp. 154–162, Sep. 2018, doi: 10.1109/JERM.2018.2841380.

5. D. S. Shumakov and N. K. Nikolova, "Fast quantitative microwave imaging with scattered-power maps," *IEEE Trans. Microw. Theory Tech.*, vol. 66, no. 1, pp. 439–449, Jan. 2018, doi: 10.1109/TMTT.2017.2697383.

6. D. Tajik, A. D. Pitcher, and N. K. Nikolova, "Comparative study of the Rytov and Born approximations in quantitative microwave holography," *Progress in Electromagnetic Research B*, vol. 79, pp. 1–19, 2017, doi:10.2528/PIERB17081003.

7. R. K. Amineh, A. Trehan, and N. K. Nikolova, "TEM horn antenna for ultra-wide band microwave breast imaging," *Progress in Electromagnetics Research B*, vol. 13, pp. 59–74, 2009, doi:10.2528/PIERB08122213

8. R. K. Amineh, J. J. McCombe, A. Khalatpour, and N. K. Nikolova, "Microwave holography using point-spread functions measured with calibration objects," *IEEE Trans. Instrumentation and Measurement*, vol. 64, no. 2, pp. 403–417, Feb. 2015, doi: 10.1109/TIM.2014.2347652.

9. D. Tajik, J. Trac, and N. K. Nikolova, "Spatial resolution evaluation of a microwave system for breast cancer screening," *2019 13th European Conf. Antennas and Propagation (EuCAP)*, Krakow, Poland, 2019, pp. 1–5.

10. D. Tajik, N. K. Nikolova, and M. D. Noseworthy, "Improving quantitative microwave holography through simultaneous use of the Born and Rytov approximations," *2019 16th European Radar Conference (EuRAD)*, Paris, France, 2019, pp. 281–284.

11. E. Lin and A. Alessio, "What are the basic concepts of temporal, contrast, and spatial resolution in cardiac CT?" *J. Cardiovasc Comput. Tomogr.* 2009, vol. 3, no. 6, pp. 403–408, doi:10.1016/j.jcct.2009.07.003.